Complex Isothermal Crystallization and Melting Behavior of Nylon 6 Nanoclay Hybrids

A. Zapata-Espinosa,[†] F. J. Medellín-Rodríguez,*[,†] N. Stribeck,[‡] A. Almendarez-Camarillo,[‡] S. Vega-Díaz,[†] B. S. Hsiao,[§] and B. Chu[§]

Centro de Investigación y Estudios de Posgrado, Facultad de Ciencias Químicas/UASLP, Av. Dr. Manuel Nava 6, Zona Universitaria, 78210, San Luis Potosí, S.L.P., México, Institut für Technische und Makromolekulare Chemie, Universitaet Hamburg, Hamburg, Germany, and Department of Chemistry, State University of New York at Stony Brook, Stony Brook, New York 11794-3400

Received February 3, 2005; Revised Manuscript Received March 5, 2005

ABSTRACT: The complex crystallization and melting behavior of neat Nylon-6 and two Nylon-6-nanoclay hybrids with different montmorillonite concentration was studied using several experimental techniques. The differential scanning calorimetry (DSC) traces were taken as a reference and experiments were made at several isothermal crystallization temperatures followed by linear heating. The results, depending on the crystallization temperature, indicated two sequences of melting for neat Nylon-6 and four for the nanoclay hybrids. After isothermal crystallization at low temperatures, neat Nylon-6 behaved different from the hybrids, however, after high crystallization temperatures there was a common melting behavior for all samples. Molecular orientation, molecular weight, and nanoclay concentration were sequentially considered in order to determine the origin of the regimes behavior in the DSC traces. Molecular weight was found as the main cause of the thermal behavior with a minimum influence of molecular orientation and nanoclay concentration. X-ray diffraction measurements indicated the formation of asymmetric γ and incomplete α and γ crystalline structures as a result of the nanoclay presence. These last structures were called truncated. Modulated melting was useful to clear mechanisms and corroborated the similar behavior for all three samples after isothermal crystallization at high temperatures. A melting mechanism was proposed on the basis of the previous behavior which involved the evolution of a quiescent low concentration morphology. This last was associated with crystallization of nonbounded macromolecules.

Introduction

Understanding the crystallization and melting behavior of quiescent thermoplastic semicrystalline polymers has been a scientific goal in the recent past, although it has also been a matter of controversy.[1−4] This situation has become complicated with the recent invention of the new thermoplastic nanostructured semicrystalline polymers, of which Nylon-6 nanoclay hybrid is a good example.[5−7] This is the first commercial nanostructured polymer, and it was created by Toyota Inc., Japan. It has shown better physical, chemical, and mechanical properties compared with the neat resin and as a consequence has generated practical and scientific interest.

Nylon-6 has been thoroughly studied in the past and it is well-known that it is able to crystallize in at least two crystalline structures, α and γ.[8] These crystal habits depend, among other factors, on the crystallization temperature and molecular weight.[8−11] Nanoclay hybrid Nylon-6 has been less studied, although it has recently been reported that the nanoclay presence favors the γ crystalline structure on shear,[12] and that the rotation of the clay platelets hinders the orientation of Nylon-6 crystals on uniaxial deformation.[13] There have also been studies on oscillatory shear where the storage and loss moduli have shown increases with nanoclay content,[14] and on X-ray morphology using solid injection-molded bars and films[15,16] where, depending on clay content, the clay platelets induced preferred orientation of the Nylon-6 crystallites.

A high number of processing operations involve the melting and crystallization steps, therefore, studies along these lines have recently been addressed. There is also scientific interest in understanding the mechanisms leading to the introduction and exfoliation of the nanoclay within the polymeric matrix. Scientific interests also include understanding the effect of temperature once the clay platelets have been introduced into the polymeric matrix. This study was made with the purpose to gain insight into the crystallization and melting behavior of Nylon-6 nanoclay hybrids, taking as a reference neat Nylon-6 and concentrating studies on the evolution of morphology after isothermal crystallization and linear heating.

Experimental Section

Materials. Neat Nylon-6 homopolymer and Nylon-6 nanoclay hybrids with 2 wt % [NCH2] and 5 wt % [NCH5] montmorillonite were synthesized by Ube Industries Inc., Japan. The synthesis in the case of hybrids was made using ϵ-caprolactam and a modified montmorillonite which was prepared via cation interchange with 12-aminolauric acid. Neat Nylon-6 had a weight-average molecular weight of 2.17 $\times$ 10^4 g/g-mol and the hybrids of 2.22 $\times$ 10^4 g/g-mol (NCH2) and 1.97 $\times$ 10^4 g/g-mol (NCH5) respectively.[14] The three samples were extruded into biaxial films. Small amounts of samples were also melted and extruded in order to obtain isotropic pellets.

Techniques. Differential Scanning Calorimetry (DSC). Differential scanning calorimetry (DSC) linear traces were obtained in a Perkin-Elmer DSC-7 calorimeter after isothermal crystallization at different temperatures. With this purpose, 7 $\pm$ 1 mg samples were placed inside an aluminum sample holder, heated at the equilibrium melting temperature of Nylon-6 (260 °C) for 3 min, fast cooled (500 °C/min nominal cooling rate) to the isothermal crystallization temperature

* Corresponding author. E-mail: francmr@uaslp.mx.
[†] Facultad de Ciencias Químicas/UASLP.
[‡] Universitaet Hamburg.
[§] State University of New York at Stony Brook.

10.1021/ma050247m CCC: $30.25
Published on Web 04/16/2005

where they remained for 30 min, and thermally scanned either at 10 or 4 °C/min up to the equilibrium melting temperature using nitrogen atmosphere.

Modulated Differential Scanning Calorimetry (MDSC). A modulated differential scanning calorimeter TA Instruments 2920 was used to collect and split the total thermal trace into the reversing and nonreversing components. All experiments were made with 7 ± 1 mg of sample within aluminum sample holders and using nitrogen atmosphere. Two types of calibrations were made, one for temperature and heat flow using indium and the other for complex heat capacity (C_p) using sapphire. After the total thermal trace (previously obtained in nonmodulated DSC) was replicated, samples were heated to the equilibrium melting temperature (260 °C) for 3 min and suddenly cooled to the isothermal crystallization temperature. There was a first nonmodulated crystallization period of 25 min followed by 5 min of modulated crystallization (i.e., quasi-isothermal crystallization with a modulation of ±0.318 °C every 60 s). This was made with the purpose to have stable modulation during heating which was made at 4 °C/min.

Wide Angle X-ray Diffraction (WAXD). X-ray diffraction measurements were made in a Siemens D5000 diffraction equipment in reflection mode using purposely prepared plaques with dimensions 1 × 1 × 0.4 cm. These specimens were prepared using stainless steel molds, Teflon, and a hot plate set at the equilibrium melting temperature. A constant weight was placed on the sample in order to eliminate air bubbles. The molten samples were suddenly quenched to 5 °C and recovered in order to introduce a pre-defined thermal history. This last step was made using a combination of two Mettler FP82HT hot stages, one of them was set at the equilibrium melting temperature (where the sample remained for 3 min) and the other at a specific crystallization temperature (where the molten sample was quickly transferred and remained for a constant period of time of 30 min). In some cases the previous process was followed by in-situ linear heating to a specific temperature, from where the sample was quenched and characterized at room temperature. The accelerating voltage was 35 kV and the filament intensity 25 mA.

Time-Resolved Small-Angle X-ray Scattering (TR−SAXS). TR−SAXS measurements were made in the A2 bending magnet beamline at HASYLAB, Germany. Samples were placed between aluminum foil and inserted into the sample chamber of a high-temperature remote controlled oven. Thermal ramps were programmed along the experimental run, SAXS data collection was carried using a one-dimensional detector and a SAXS data collection computing code. The experimental data were calibrated with rat tendon and corrected for background and dark current.

SAXS Theory and Calculations

SAXS results were used to calculate the corresponding morphology. For calculation purposes, it was convenient to apportion the scattering reciprocal space curve into three regions, low, intermediate, and high q. To extrapolate data in the low q side, the Debye model[17] was used. This is given by $I(q)|_{q\to 0} = A/(1 + \epsilon^2 q^2)^2$, where A is a constant and ϵ is an inhomogeneity length. This model was used to generate the extrapolated $I(q)|_{q=0}$. The intermediate q range was well-defined, and polynomial smoothing of the scattering data was enough in order to minimize experimental deviations. The high $I(q)|_{q\to\infty}$ side was corrected for deviations from an ideal two-phase system given by Porod's law. For this purpose, the ideal intensity was corrected with $I_{ID} = I(q) - I_b(q)/H^2(q)$. Here $I_b(q)$ is the background intensity due to density fluctuations within the phases and $H^2(q)$ is a smoothing function which takes into account the interface thickness. The background intensity was considered polynomial[18] and was subtracted from the experimental data; the smoothing function was assumed to be sigmoidal.[19] The corrected intensity was extrapolated at high q values in order to locate Porod's region. This generated the $G_1(q)$ interface function[20] given by $G_1(q) = I_P q^4 - I(q)q^4$, which was used to calculate the interface distribution through

$$g_1(r) = \frac{t}{2\pi^2 V}\int_0^\infty G_1(q)\cos(qr)\,dq \qquad (1)$$

where t is the sample thickness and V is the volume occupied by lamellar stacks.

Results

Isothermal Crystallization and Melting. Understanding the crystallization behavior of polymers has been closely related to understanding the melting mechanisms.[1−4] Both viewpoints are considered complementary,[1] and it has recently become common to first introduce a defined thermal history to samples and, on the basis of the melting results, give an explanation to the crystallization process. Using this strategy, we have reported before[11] that quiescent crystallization (and melting) of Nylon-6 homopolymers is strongly dependent on molecular weight. Low molecular weight Nylon-6 develops three sequences of melting and high molecular weight five sequences and a transition zone. Despite the fact that that it starts with the γ form at very low crystallization temperatures, low molecular weight Nylon-6 immediately shows a $\gamma-\alpha$ crystal transition at intermediate temperatures, this is then followed by the development of the α crystalline structure at high temperatures. High molecular weight on the other hand first starts with the γ form at low crystallization temperatures, it reaches the $\gamma-\alpha$ transition and ends up with the α crystal habit at high crystallization temperatures. On linear heating, the unstable γ structure is able to recrystallize to the most stable α form and crystals follow up steplike melting mechanisms.[11]

Nylon-6 hybrids consist of macromolecules which are chemically attached (end-tethered) to the nanoclay surface;[5,22] therefore, different crystallization and melting mechanisms should be expected regarding neat Nylon-6. Figure 1 shows the DSC melting traces of the neat Nylon-6 used in this study where the typical behavior of low molecular weight Nylon-6 is present,[11] although only two sequences of melting, the first (80−190 °C) and second (195−200 °C), are observed. The first sequence starts at low temperatures (80 °C) and involves the formation and evolution of triple melting behavior. In this case, the melting endotherms change in magnitude and position until the convolution of the second and third endotherms takes place at 195 °C, where another melting sequence starts. Although not shown here, during a third melting sequence all endotherms become convoluted, giving place to a single peak which then moves to higher temperatures. This behavior has been observed before in poly(ethylene terephthalate) (PET).[21] NCH2 behaves in a different manner, as shown in Figure 2. It strongly resembles however high molecular weight Nylon-6 since it shows four sequences of melting and a transition zone. The first sequence (80−160 °C) involves a recrystallization exotherm and double melting behavior with the third endotherm decreasing as the second increases. The second sequence (160−175 °C) reverses the last one; i.e., the third endotherm increases and the second decreases. It also gives rise to a new endotherm at temperatures close to the recrys-

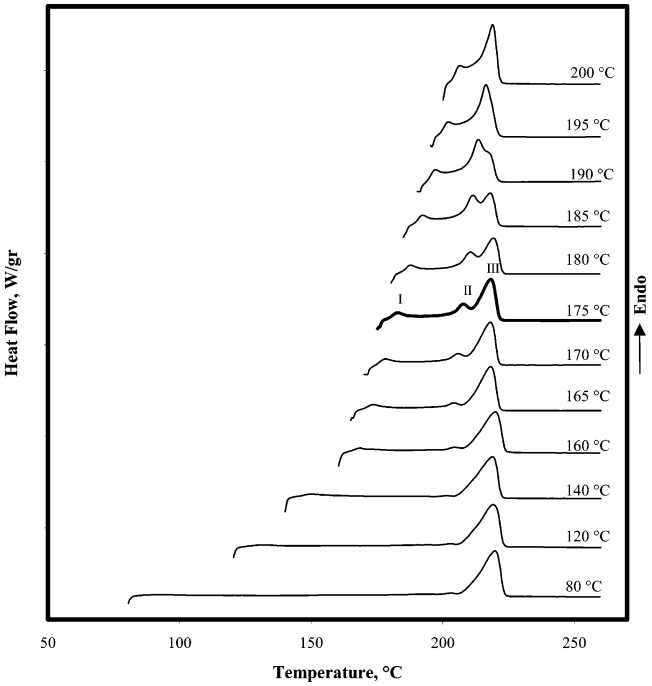

Figure 1. Linear heating DSC traces of neat reference Nylon-6 after isothermal crystallization ($T_m°$ = 280 °C, 3 min; t_c = 30 min). Crystallization temperatures are shown.

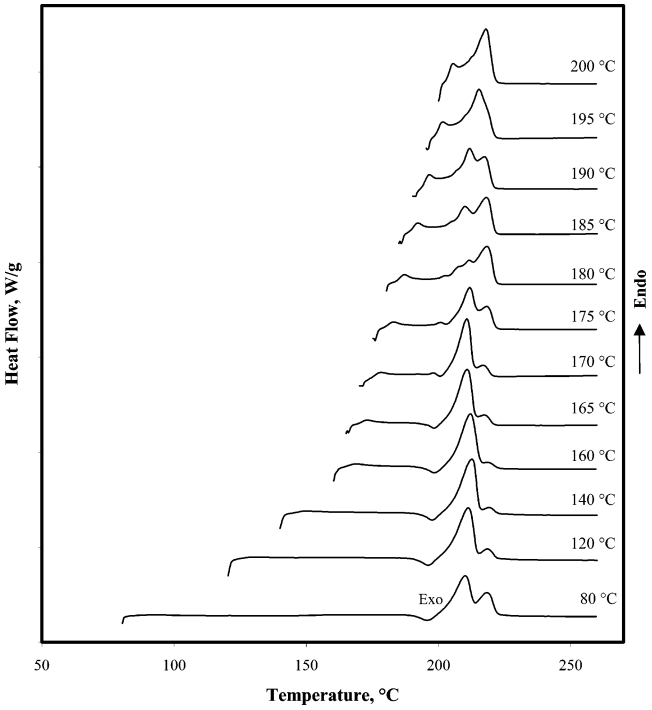

Figure 2. Linear heating DSC traces of NCH2 after isothermal crystallization. ($T_m°$ = 280 °C, 3 min; t_c = 30 min). Crystallization temperatures are shown.

tallization exotherm. Then follows a transition temperature (180 °C), where up to five melting endotherms are observed. The third sequence (185−190 °C) is the typical evolution of triple melting behavior and during the fourth sequence (195−200 °C), there must be the convolution of endotherms I and II just as in neat Nylon-6. There should be a last sequence (not shown) where all endotherms, once convoluted into a single one, will move to higher temperatures. NCH5 only shows small changes regarding NCH2 as indicated in Figure 3; for

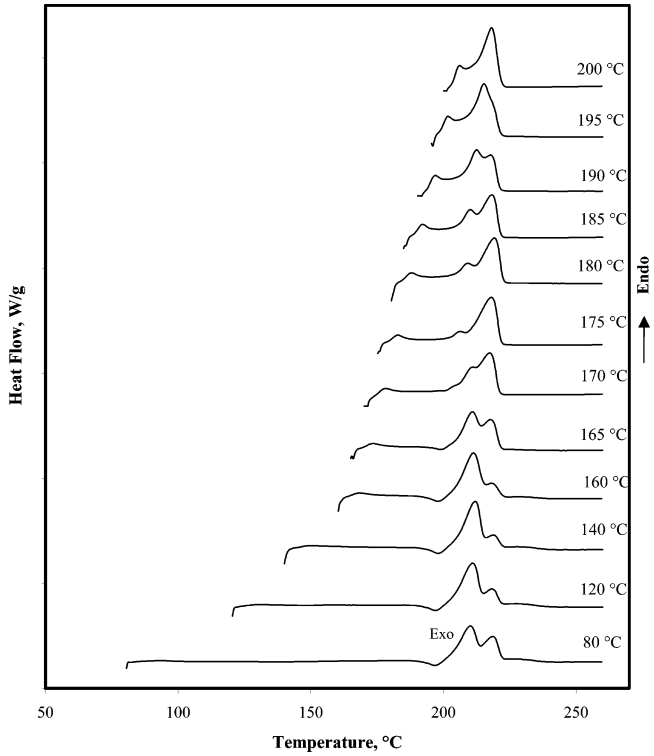

Figure 3. Linear Heating DSC traces of NCH5 after isothermal crystallization. ($T_m°$ = 280 °C, 3 min; t_c = 30 min). Crystallization temperatures are shown.

example, the transition temperature is located 10 °C below (170 °C), and it only has four melting endotherms.

Discussion

The previous DSC results could be wrongly interpreted. For instance, they could be seen as an indication that the nanoclay presence is motivating the differences in thermal behavior. Worse, one may be led to conclude that the effect of nanoclay is equivalent to the previously reported effect of molecular weight[11] since thermal evolutions are quite similar. However, considering the origin of samples, and also the complex nature of Nylon-6 nanoclay hybrids, such effects as molecular orientation had to be considered before attempting conclusions regarding the molecular weight and the nanoclay presence.

Neat Nylon-6 and the hybrid samples were originally in biaxial stretched film form. Therefore, in spite that molecular orientation was considered to have been eliminated during the melting period, it was also realized as a possibility affecting the thermal traces. Although not shown here, we generated comparative thermal results of samples in isotropic (pellet) and bioriented film forms, after erasing thermal history in the molten state (using the same period of time in the melt) and linear heating. The results did not indicate differences between both types of samples. Therefore, processing-related molecular orientation was discarded as being a factor that influenced the thermal traces. It then remained to consider molecular weight and nanoclay presence as the two other potential causes influencing the DSC results.

A nanoclay hybrid consists of homogeneously distributed end-tethered macromolecules to the nanoclay platelets which act as cross-linkers in the whole polymeric matrix.[5] The synthesis mechanism first involves

the molecular fixation of the ion onium on the nanoclay surface through ion interchanges. This is followed by the formation of an initial complex resulting from the reaction between an amino acid initiator and ϵ-caprolactam and then by the preferential polymerization of the rest of monomers at the tip of the carboxylic side of the tethered complex.[22] This process does not impede however the quiescent polymerization of monomers which are not chemically bonded to the nanoclay surface, particularly if there is a high concentration of initiator. Therefore, and depending on the nanoclay concentration, a mixture of tethered/nontethered macromolecules should be expected as the most probable polymerization product. In other words, if the initiator concentration is low, there is a higher probability of nanoclay chemical bonding to the nanoclay surface.

A form to test the proposition of molecular weight as the cause of the observed thermal behavior is to compare the X-ray diffraction behavior of samples in terms of the formation of different crystal structures as a function of the crystallization temperature. As reported before,[11] and cited here for clearness, low molecular weight Nylon-6 develops γ habits at low crystallization temperatures, then, immediately changes to the $\gamma-\alpha$ transition and then again to the most stable α form at slightly higher crystallization temperatures. High molecular weight Nylon-6 on the other hand starts with the γ form, remaining in this form within a wider range of crystallization temperatures, and then switches to the stable α form at high isothermal crystallization temperatures. We specifically selected three isothermal crystallization temperatures in this study and obtained the WAXD patterns of samples afterward: low (80 °C), intermediate (175 °C), and high (200 °C) crystallization temperatures. The results in Figure 4 indeed corroborate the molecular weight proposition since there is a proportional behavior between reference Nylon-6 and the hybrids regarding the formation of crystal habits. For example, the diffraction results of neat Nylon-6 in Figure 4a indicate that, after isothermal crystallization at 80 °C, and due to the low molecular weight, Nylon-6 crystals consist of a mixture of γ/α habits (i.e., they are already at the crystal transition). In addition, at intermediate (175 °C) and high (200 °C) crystallization temperatures, there is the expected change to the stable α form, which shows the two (200), (002)/(202) diffracting peaks, although these are in disproportion respect to each other as an indication of the development of imperfect α crystals during crystallization.

NCH2 started with the unstable although asymmetrical γ form at 80 °C, as shown in Figure 4b, characteristic of high molecular weight Nylon-6. However, at intermediate crystallization temperatures (175 °C), NCH2 crystals developed a mixture of atypical truncated crystalline structures (i.e., crystalline structures with the lack of a family of diffracting planes) of both γ and α crystals.[23] In other words, the (001)-γ diffracting plane is causing low diffraction (generating γ_t), and the (200)-α plane is not present anymore. At high crystallization temperatures (200 °C) there is only truncated α_t which shows a unique (002)/(202) diffracting peak.

NCH5 also starts (80 °C) with asymmetrical γ habits due to the high molecular weight as shown in Figure 4c, although, as expected, and due to the lower molecular weight than NCH2, it immediately develops truncated α_t at the same crystallization temperature (175 °C) where NCH2 had still two crystal habits. In summary, the previous behavior is in correlation with the molecular weight, such as in Nylon-6 homopolymers.[11] Therefore, the thermal results must also be due to the molecular weight and indicate that NCH2 must have higher molecular weight than NCH5 (as reported),[14] since, under identical crystallization conditions, the second melting endotherm is higher in the first case;[11,21] nevertheless, this difference must not be very pronounced based on the appearance of the thermal traces.

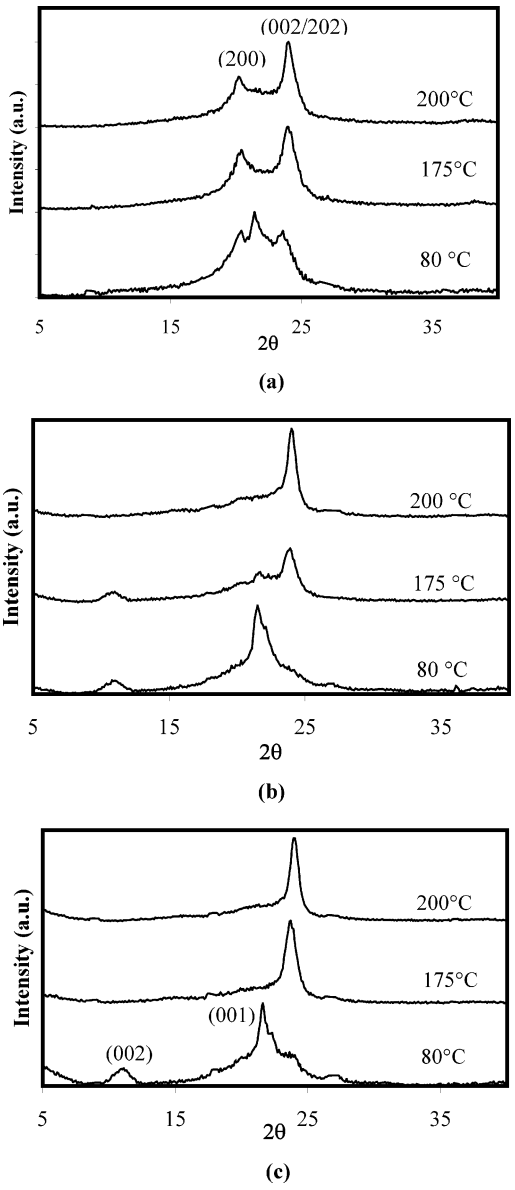

Figure 4. WAXD patterns after isothermal crystallization (30 min) at the indicated crystallization temperatures: (a) Nylon-6; (b) NCH2; (c) NCH5.

On the basis of the previous results, the nanoclay effect can also be figured, it does not strongly influence the thermal traces but gives rise to distorted (asymmetrical γ) and truncated $\alpha-\gamma$ crystalline structures, whose origin will be discussed in the nest sections. In addition, the nanoclay concentration evidently promotes the formation of α_t.

Modulated Melting Behavior. As shown before with the conventional DSC results, Nylon-6 and nanoclay hybrids behaved different on melting after isother-

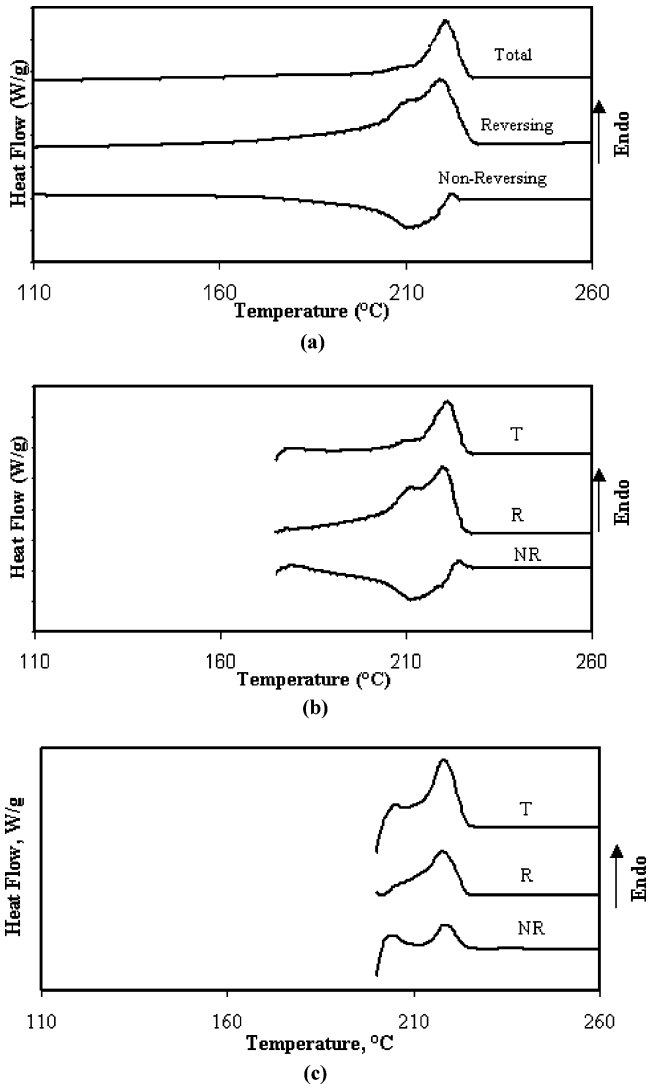

Figure 5. MDSC traces of Nylon-6 after isothermal crystallization (30 min): (a) 80 °C; (b) 175 °C; (c) 200 °C.

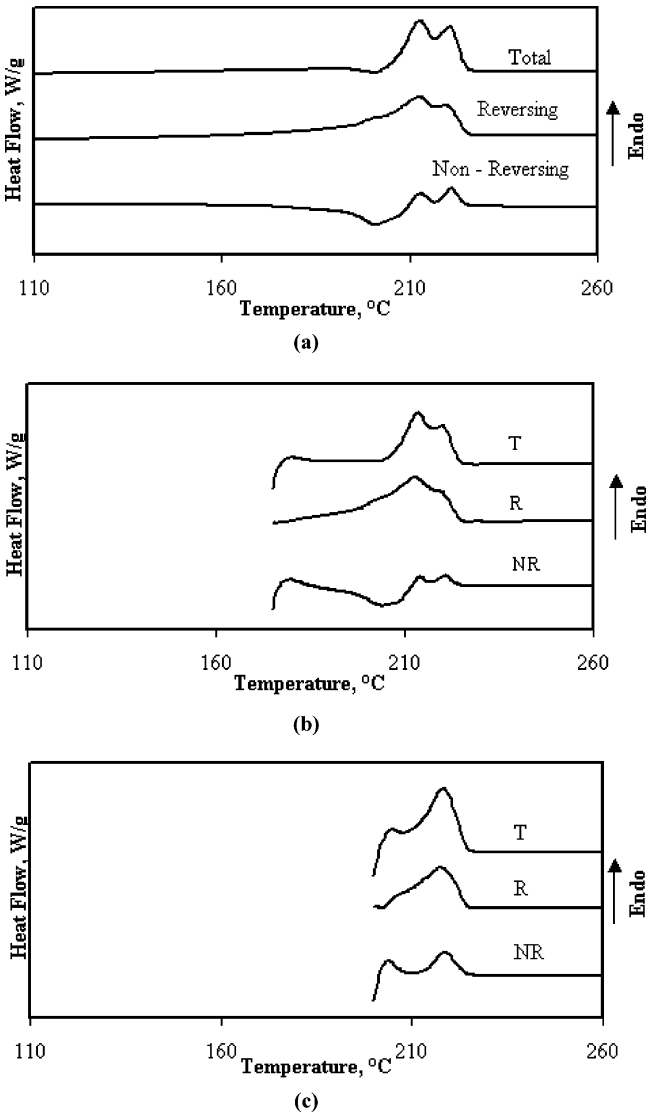

Figure 6. MDSC traces of NCH2 after isothermal crystallization (30 min): (a) 80 °C; (b) 175 °C; (c) 200 °C.

mal crystallization at low temperatures; however, they behaved similarly on melting after isothermal crystallization at high temperatures. Therefore, to generate information on the melting mechanisms, modulated melting experiments, whose results are shown in Figures 6-8, were made after low (80 °C), intermediate (175 °C), and high (200 °C) crystallization temperatures.

Figure 5a indicates that after isothermal crystallization at low temperature (80 °C), Nylon-6 develops a total melting signal (associated with the original mixture of γ and α crystal habits) which divides itself into a double melting reversing and a nonreversing trace consisting of a recrystallization exotherm and an a small melting endotherm. In the nonreversing trace, the recrystallization exotherm is in the same position as the first reversing melting endotherm and so a parallel melting and recrystallization process must be taking place. The nonreversing recrystallization exotherm and the reversing second melting endotherm seem to correspond each other in magnitude; therefore, it can be proposed that the recrystallized crystals melt at this endotherm in a similar manner as proposed before for PET.[1] As for the small nonreversing melting endotherm, it can be assigned to melting of a fraction of stable (most probably α) isothermal crystals in a combination that leads to a dual (reversing/nonreversing) melting process of isothermal crystals. After isothermal crystallization at intermediate temperatures (Figure 5b; 175 °C), the previous process still takes place, although, the recrystallization exotherm is slightly smaller due to the higher crystallization temperature. After high crystallization temperatures (Figure 5c; 200 °C) the melting behavior changes; there is now an apparently unique reversing and two nonreversing melting endotherms whose origin is the topic of current research.[24]

NCH2 shows a complex and different melting behavior in Figure 6. After isothermal crystallization at low temperature (Figure 6a; 80 °C), there are three reversing melting endotherms and, after the nonreversing recrystallization exotherm (which coincides with the total recrystallization exotherm), there is a dual nonreversing melting sequence. A different explanation should thus be expected regarding the melting process of neat Nylon-6. As indicated before, the first reversible melting endotherm, i.e., the one coincident with the nonreversing recrystallization exotherm, can be assigned to a population that melts and recrystallizes to either more perfect or thicker crystals. The second reversing endotherm could then be assigned to melting (and recrystallization) of γ crystals into the more stable α form, phenomenon observed before with neat Nylon-

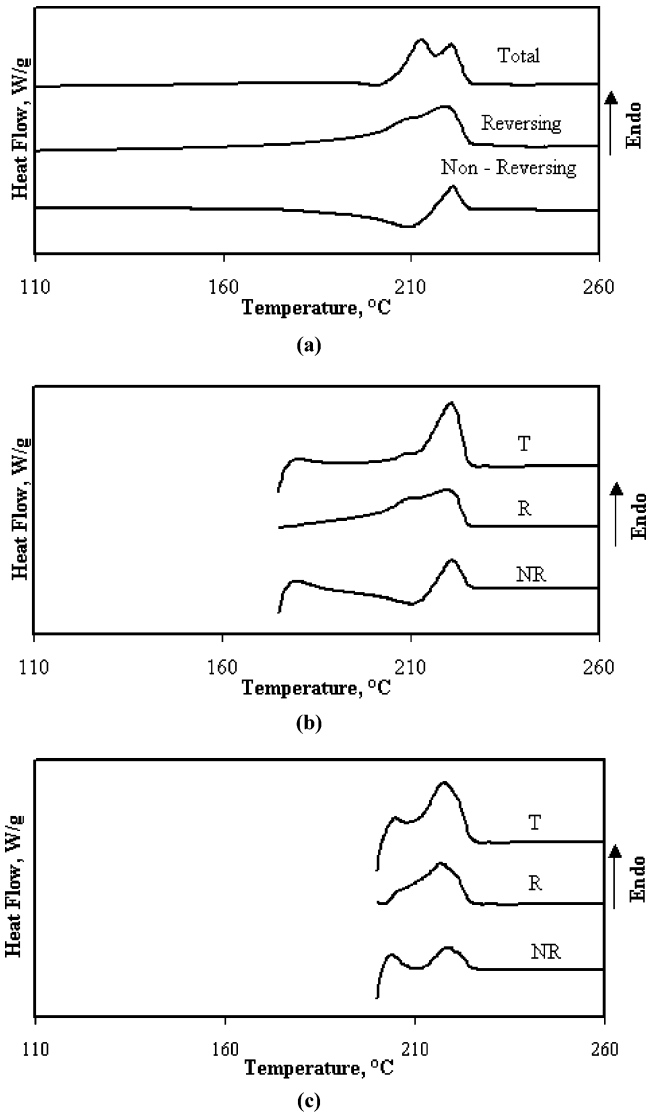

Figure 7. MDSC traces of NCH5 after isothermal crystallization (30 min): (a) 80 °C; (b) 175 °C; (c) 200 °C.

6.[11] The third endotherm can as a consequence be associated with melting of the recrystallized crystals (i.e., those that thickened, or perfected, or recrystallized to a different form on heating). Interestingly, there are two nonreversing melting endotherms which are located in the same positions as the second and third reversible endotherms. If we assume the explanation given before for Nylon-6, and also proposed for PET,[1] one of the endotherms can be associated with nonreversing primary stable γ crystals (first endotherm) and the other to primary stable α crystals (second endotherm). Melting after intermediate crystallization temperatures (Figure 6b; 175 °C) supports the previous proposition since there is still the same behavior but now the sample started with a mixture of truncated α/γ crystals. Remarkably, after crystallization at higher temperatures (Figure 6c; 200 °C) the melting process follows up the same behavior as neat reference Nylon-6 including the apparent formation of two nonreversing melting endotherms.

As shown in Figure 7a, after isothermal crystallization at 80 °C, NCH5 displayed modulated reversing/nonreversing thermal traces which were closer to Nylon-6 than to NCH2. This was the case despite the facts that the total melting trace was closer to NCH2 than

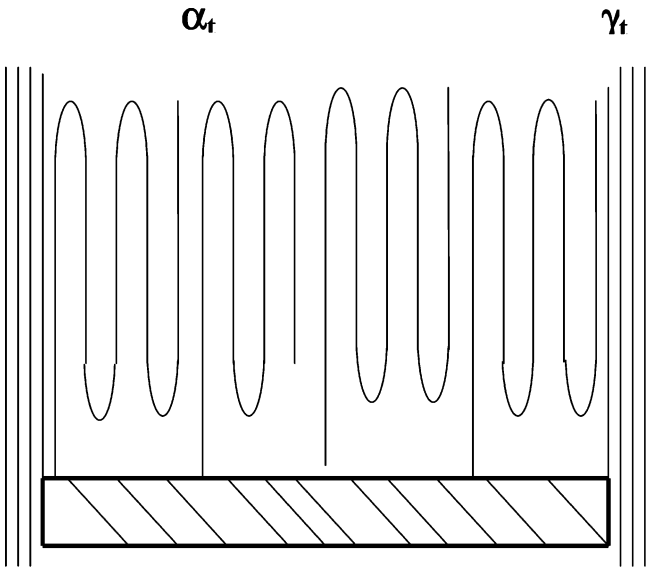

Figure 8. Proposed crystallization scheme to explain the formation of α_t and γ_t.

to Nylon-6, and that the asymmetric γ form (molecular weight promoted) was also present at the beginning of the heating process (just as in NCH2). To explain the NCH5 behavior on melting, we need to take into account that, due to the lower nanoclay content, NCH2 has a higher probability of forming two morphologies. One of these must be associated with bounded (end-tethered macromolecules oriented along the substrate normal direction) and the other to nonbounded (isotropic) macromolecules (see SAXS results later). From the higher concentration bounded phase, the stable α (truncated) and the stable γ (truncated) crystals must emerge. The stable α_t, involving hydrogen bonds between antiparallel chains, can be achieved by adjacent reentry of folded chains into the crystals,[25] and must be originated on crystallization of the bulk end-tethered chains. On the other hand, the stable γ_t (extended-like chains), involving hydrogen bonding between parallel chains, can originate on the edges of the previous crystals which are in contact with the isotropic phase, i.e., in the interface of the isotropic and oriented phases, as shown in Figure 8. In NCH5 however, most of the macromolecules are end-tethered to the nanoclay surface due to the higher nanoclay concentration, rendering as a consequence a single morphological population (α_t). In this form, although the total melting signal looks similar to NCH2, the melting process is different and the melting/recrystallization step must only involve perfecting and thickening processes without $\alpha-\gamma$ transformations, rendering as a consequence a single nonreversing melting endotherm. Increasing the crystallization temperature (Figure 7b; 175 °C) does not make any important difference due to the nature of the original crystals and, once again, after isothermal crystallization at high temperatures (Figure 7c; 200 °C) the melting characteristics of NCH5 are very similar to those of neat Nylon-6 and NCH2.

In Situ Studies. Comparing the diffraction and thermal results in Figures 4−7, it is easy to figure that the temperature with the most important contrast is 175 °C. Therefore, being the purpose to sustain the explanations given before, we used this temperature to systematically analyze the melting process in terms of WAXD with the fast cooling technique (21) and in terms of SAXS with time-resolved in situ measurements.

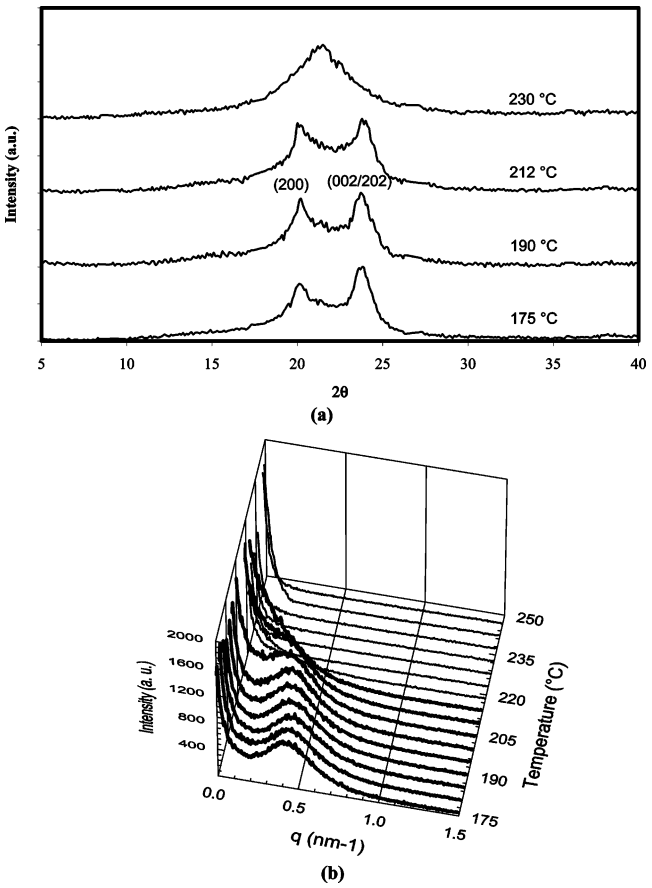

Figure 9. (a) WAXD patterns on simulated melting of Nylon-6; (b) in situ SAXS patterns on melting. ($T_m°$ = 280 °C; 3 min, T_c = 175 °C.)

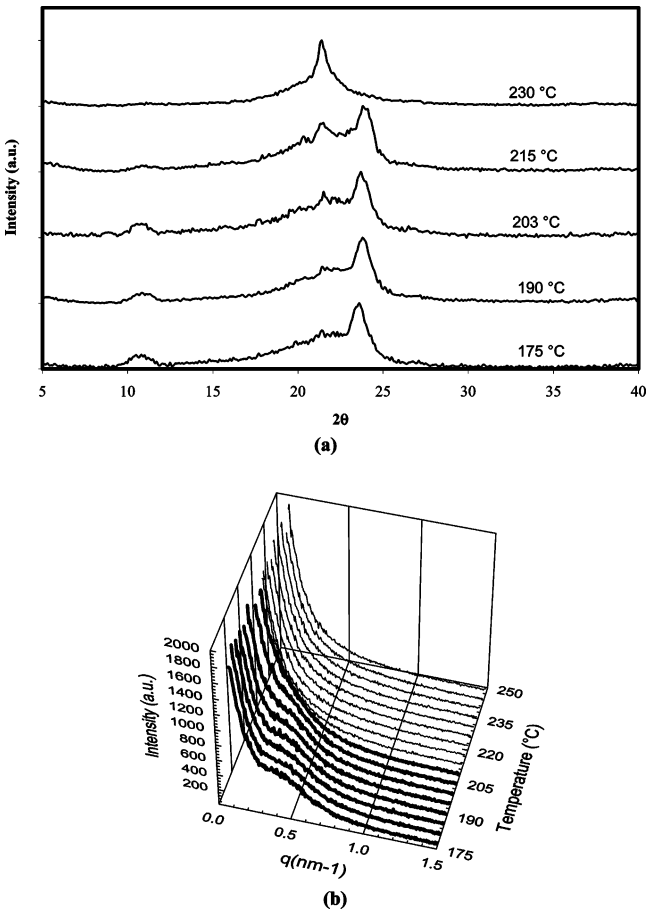

Figure 10. (a) WAXD patterns on simulated melting of NCH2; (b) in situ SAXS patterns on melting of NCH2. ($T_m°$ = 280 °C; 3 min, T_c = 175 °C.)

Table 1. SAXS Results for: (a) Nylon-6 under Heating after Isothermal Crystallization ($T_m°$ = 280 °C, 3 min; t_c = 30 min; 175 °C) and (b) NCH2 (Identical Conditions) (L = Long Spacing; r_1 = Crystal Thickness; r_2 = Amorphous Thickness)

heating temp (°C)	L (nm)	r_1 (nm)	r_2 (nm)
	(a)		
175.0	9.0	4.1	4.9
179.7	9.2	4.1	5.1
198.6	9.6	4.4	5.2
203.3	9.6	4.4	5.2
208.1	9.8	4.5	5.3
212.8	9.9	4.6	5.3
217.5			
	(b)		
175.0	9.0	4.0	5.0
179.7	9.1	4.1	5.0
198.6	9.5	4.2	5.1
203.3	9.7	4.4	5.3
208.1	9.8	4.5	5.3
212.8			

Figure 9a shows the WAXD thermal evolution of Nylon-6 which, after isothermal crystallization at 175 °C, indicates the formation of relatively imperfect α crystals. However, as the heating process succeeds, there is some crystal perfection between 175 and 190 °C (the (200) crystal peak increases its definition). This step is finally followed by sudden melting of the α structure after 212 °C. The MDSC results In Figure 6 had indicated reversible melting in parallel with nonreversing recrystallization occurring at temperatures close to 212 °C. Therefore, at least part of the nonreversing recrystallization should be considered associated with crystal perfection. In situ SAXS experiments are shown in Figure 9b for the neat reference Nylon-6. This behavior is well-known, upon crystallization, there is the initial formation of a maximum which then slightly moves to lower q values as the crystallization time increases indicating lamellar thickening (see also Table 1), a process that must be at least part of the nonreversing recrystallization exotherm.

The WAXD melting behavior of NCH2, after isothermal crystallization at 175 °C, produced different patterns, as shown in Figure 10a. During linear heating, the original truncated γ_t/α_t crystalline structures remained basically the same up to 203 °C, with an almost unnoticed perfecting process. However, as temperature increases farther, the unstable part of γ_t is converted into α_t. As for α_t, it should directly be divided into stable/unstable crystals. Melting takes place above 215 °C rendering a peak associated with the amorphous background (sharper than in Nylon-6 due to the substrate-oriented melt). Considering the propositions given in terms of the MDSC results for NCH2, the pronounced nonreversing recrystallization exotherm should then be related to perfecting, reorganization to a different crystalline structure and lamellar thickening of the isotropic phase (see also Table 1). The SAXS results shown in Figure 10b indeed showed a maximum, this had however much lower intensity than Nylon-6 and as a consequnce was considered associated with a smaller fraction of quiescent (nonbounded) crystals since it basically displayed the same melting characteristics as neat nylon-6.

The simulated WAXD melting process of NCH5, as expected, was the simplest. As shown in Figure 11a,

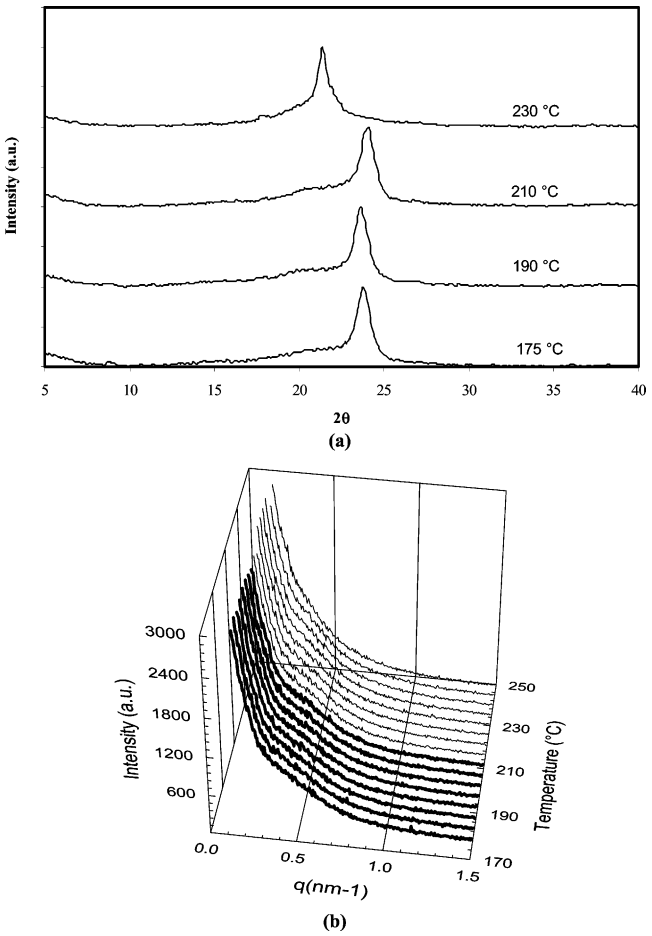

Figure 11. (a) WAXD patterns on simulated melting of NCH5; (b) in situ SAXS patterns on melting of NCH5. ($T_m°$ = 280 °C; 3 min, T_c = 175 °C.)

there was only the α_t crystalline structure after isothermal crystallization at 175 °C, without any important change as the heating temperature increased. Considering the presence of a single-crystal habit, the nonreversing recrystallization process should be considered associated with perfecting and lamellar thickening. The SAXS results in Figure 11b indicated, as expected, and in close correspondence with the SAXS results of NCH2, that the amount of quiescent crystals is minimum giving place to an almost imperceptible scattering maximum.

Conclusions

After molecular orientation and nanoclay concentration were discarded as influencing the thermal results of Nylon-6 and Nylon-6 nanoclay hybrids, it was concluded that the differences in thermal behavior were mainly due to the molecular weight.

After low and intermediate isothermal crystallization temperatures, melting characteristics were different for neat reference Nylon-6, however, after isothermal crystallization at high temperatures melting characteristics were similar to those of the hybrids.

The formation of γ and α crystal structures took place in the nanoclay hybrids with two important differences, crystals generated asymmetrical γ diffraction patterns and, under some circumstances, crystals developed atypical truncated crystalline structures (i.e., crystalline structures with lack of a family of diffracting planes).

The complex crystallization mechanism of hybrids could be explained on the basis of a crystallization model previously proposed for PET.

There was a small fraction of isotropic nonbounded crystals in the nanostructured hybrids which had the same melting characteristics as neat nylon-6. The amount of the isotropic fraction was low and its concentration changed inversely with the nanoclay content.

Acknowledgment. The support of the National Research Council of Science and Technology (CONACyT) in Mexico through Grants 39638-Y and U40177-K and the support of the FRC and Promep-CA9/FCQ of the Autonomous University of San Luis Potosí, Mexico are greatly appreciated.

References and Notes

(1) Avila-Orta, C. A.; Medellín-Rodriguez, F. J.; Wang, Z. G.; Navarro-Rodriguez, D.; Hsiao, B. S.; Yeh, F. *Polymer* **2003**, *44*, 1527−1535.
(2) Roberts, R. C. *J. Polym. Sci., Polym Lett.* **1988**, 28−32.
(3) Basset, D. C.; Olley, R. H.; Al Raheil, R. A. H. *Polymer* **1988**, *29*, 1745−1754.
(4) Al Raheil, I. A. M. *Polym. Int.* **1994**, *35*, 189−195.
(5) Okada, A.; Kawasumi, M.; Kurauchi, T.; Kamigaito, O. *Polym. Prepr. (Am. Chem. Soc., Div. Polym. Chem.)* **1987**, *28*, 447−448.
(6) Kojima, Y.; Okada, A.; Usuki, A.; Kawasumi, M.; Kurauchi, T.; Kamigaito, O.; Deguchi, R. *Polym. Prepr. Jpn.* **1990**, *39*, 2430−2435.
(7) Kojima, Y.; Usuki, A.; Kawasumi, M.; Okada, A.; Fukushima, Y.; Kurauchi, T.; Kamigaito, O. *J. Mater. Res.* **1993**, *8*, 1185−1189.
(8) Gianchandani, J.; Spruiell, J. E.; Clark, E. S. *J. Appl. Polym. Sci.* **1982**, *27*, 3527−3551.
(9) Arakawa,, T.; Nagatoshi, F.; Arai, N. J. *Polym. Sci., Part A-2* **1969**, 1461−1472.
(10) Gurato, G.; Fichera, A.; Grandi, F. Z.; Zannetti, R.; Canal, P. *Makromol. Chem.* **1974**, *175*, 953−975.
(11) Medellín-Rodríguez, F. J.; Larios-López, L.; Zapata-Espinosa, A.; Phillips, P. J.; Dávalos-Montoya, O.; Lin, J. S. *Macromolecules* **2004**, *37*, 1799−1809.
(12) Medellín Rodríguez, F. J.; Burger, C.; Hsiao, B.; Chu, B.; Vaia, R.; Phillips, S. *Polymer* **2001**, *42*, 9015−9023.
(13) Medellín-Rodriguez, F. J.; Hsiao, B. S.; Chu, B.; Fu, X. *J. Macromol. Sci., Part B: Phys.* **2003**, *B42*, 201−214.
(14) Krishnamoorti, R.; Giannelis, P. E. *Macromolecules* **1977**, *30*, 4097−4102.
(15) Kojima, Y.; Usuki, A.; Kawasumi, M.; Okada, A.; Kurauchi, T.; Kaji, K. *J. Polym. Sci., Part B: Polym. Phys.* **1995**, *33*, 1039−1045.
(16) Kojima, Y.; Usuki, A.; Kawasumi, M.; Okada, A.; Kurauchi, T.; Kaji, K. *J. Polym. Sci., Part B: Polym. Phys.* **1994**, *32*, 625−630.
(17) Debye, P.; Anderson, H. R., Jr.; Brumberger, H. *J. Appl. Phys.* **1957**, *28*, 679−673.
(18) Vonk, C. G. *J. Appl. Crystallogr.* **1973**, *6*, 81−86.
(19) Ruland, W. *J. Appl. Crystallogr.* **1971**, *4*, 70−77.
(20) Ruland, W. *Colloid Polym. Sci.* **1977**, *255*, 417−427.
(21) Medellin-Rodriguez, F. J.; Phillips, P. J.; Lin, J. S.; Campos, R. *J. Polym. Sci., Part B: Polym. Phys.* **1997**, *35*, 1757−1774.
(22) Okada, A.; Usuki, A. *Mater. Sci. Eng.* **1995**, *C3*, 109−115.
(23) Wu, T.-M.; Chen, E.-Ch.; Liao, Ch.-S. *Polym. Eng. Sci.* **2002**, *42*, 1141−1150.
(24) Medellin-Rodriguez, F. J.; Perez-Chantaco, A. To be published.
(25) Holmes, R.; Bunn, D. W.; Smith, D. J. *J. Polym. Sci.* **1955**, *17*, 159−177.

MA050247M